Combined cathodoluminescence spectroscopy, electron microprobe and laser ablation ICP mass spectrometry analysis: an attempt to correlate luminescence and chemical composition of monazite

(Article begins on next page)

25 December 2024

UNIVERSITÀ DEGLI STUDI DI TORINO

Vaggelli, G., Cossio, R., Petrelli, M., Rossetti, P., 2008. Combined cathodoluminescence spectroscopy, electron microprobe and laser ablation ICP mass spectrometry analysis: an attempt to correlate luminescence and chemical composition of monazite. Microchimica Acta, 161 (3-4), 313-321.

COMBINED CL SPECTROSCOPY, EPMA AND LA-ICPMS ANALYSIS: AN APPROACH TO TENTATIVELY CORRELATE LUMINESCENCE AND CHEMICAL COMPOSITION ON MONAZITE FROM DORA MAIRA MASSIF (ITALY).

Gloria Vaggelli[1], Roberto Cossio[2], Maurizio Petrelli[3] and Piergiorgio Rossetti[2]

1)CNR - Istituto di Geoscienze e Georisorse, Via V. Caluso 35, I-10123 Torino, Italy.
2)Dipartimento di Scienze Mineralogiche e Petrologiche, Via V. Caluso 35, Torino, Italy.
3) Dipartimento di Scienze della Terra, Piazza dell'Università, Perugia, Italy.

Corresponding author:

Roberto Cossio
Dipartimento di Scienze Mineralogiche e Petrologiche, Via V. Caluso 35, Torino, Italy.
Email: roberto.cossio@unito.it

1

COMBINED CL SPECTROSCOPY, EPMA AND LA-ICPMS ANALYSIS: AN APPROACH TO TENTATIVELY CORRELATE LUMINESCENCE AND CHEMICAL COMPOSITION ON MONAZITE FROM DORA MAIRA MASSIF (ITALY).

G. Vaggelli[1], R. Cossio[2], M. Petrelli[3] and P. Rossetti[2]

1)CNR - Istituto di Geoscienze e Georisorse, Via V. Caluso 35, I-10123 Torino, Italy.
2)Dipartimento di Scienze Mineralogiche e Petrologiche, Via V. Caluso 35, Torino, Italy.
3) Dipartimento di Scienze della Terra, Piazza dell'Università, Perugia, Italy.

Key Words: monazite, LA-ICPMS analysis, monochromatic cathodoluminescence, panchromatic cathodoluminescence, Dora Maira.

ABSTRACT

Quantitative electron microprobe analyses, cathodoluminescence (CL) panchromatic images and monochromatic spectra, as well as LA-ICPMS analyses of minor and trace elements were performed on selected monazite crystals from Dora Maira Massif, Western Alps (Italy).

BSE images suggest no patchy or chemical zoning or strong disomogeneity.

The electron microprobe (EPMA) data indicate that the crystals are Ce-monazite with a mostly homogeneous composition in major elements (LREE). Low (far below 1 wt%) and variable Th, Ca and Y contents were detected.

The laser ablation (LA-ICPMS) data indicate that all HREEs occur as minor or trace elements (from thousand to few ppm). Interesting Si, Sr, U and Pb concentrations are also detected. Th, Y and Ca values are comparable to EPMA data.

The use of panchromatic and monochromatic cathodoluminescence images with cathodoluminescence spectra in combination with microanalytical techniques suggest that the luminescence of monazite is mostly due to four bands centered at 316, 339, 634 and 683, partially overlapping and not clearly related to impurity activators or to microchemical differences. However, we can tentatively attribute the first two bands to Gd^{3+} and Ce^{3+}, respectively. In addition, several minor peaks centered at 384, 411, 485, 498, 562 and 596 nm also occur in between. These minor peaks may be tentatively assigned to Tb^{3+}, Dy^{3+} and Sm^{3+}.

INTRODUCTION

Monazite is a rare-earth-element phosphate mineral that is present as an accessory mineral phase in many igneous and metamorphic rocks. It has the nominal composition (LREE) PO_4 and the LREEs (primarily La + Ce + Nd) generally comprise approximately 75% of the total cation proportions (exclusive of P) of most metamorphic monazites (Spear & Pyle, 2002). Th, Ca, Y and Si may also occur as major elements moving the monazite compositions towards brabantite $(CaTh[PO_4]_2)$ or huttonite $(ThSiO_4)$ end-members or xenotime (YPO_4). Most monazite contain as minor or trace elements HREEs, Y, Th, Ca, Si, U and finally Pb: the latter of radiogenic origin due to Th and U decay (Parrish, 1990).

A tentative attempt was made to find out the main CL features of this rock accessory minerals whose importance is growing for U-Th-Pb geocronology of moderate to high-grade metamorphic rocks. Indeed, monazite grows as a metamorphic mineral over a broad stability range, possesses a high closure temperature and finally is quite resistant to alteration of Pb isotopes by solid-state diffusional exchange (Parrish, 1990, Suzuchi et al., 1994, Harrison et al., 2002, Cherniak et al., 2004).

The main objective of this paper is to present and discuss the CL properties of "normal" and most widespread Ce-monazites (Foster 1998) in relation with their chemical compositions.

CL microscopy and microanalysis are now routinely used for the analysis of structural defects and impurities in a wide range of minerals.

Scanning electron microscope (SEM) can be used for cathodoluminescence (CL) microscopy and spatial resolved CL spectroscopy by means of a light collector and monochromator. The luminescence emission bands are "activated" by impurity and/or atom defects, and the emission features can be characteristic of that particular activator (Remond et al., 2000).

EXPERIMENTAL

Panchromatic and Monochromatic CL analysis

CL images and spectra were performed by an Oxford MONO CL mounted on a Stereoscan S- 360 SEM of Cambridge Instruments equipped with an MMR Technoligies cold stage sample holder.

CL panchromatic and monochromatic images were acquired at a probe current of 5nA, an accelerating potential of 15 kV and working distance of 16 mm.

CL spectra were first collected, on spot areas, at room temperature from 250 to 800 nm with a resolution of 5nm and a sampling time of 1s. A probe current of 5nA, an accelerating potential of 15 kV and working distance of 16 mm were also applied.

CL spectra on monazite 1 and 4 were finally carried out at higher resolution (1nm), probe current (10 nA) and accelerating potential (30 kV), both at room and Liquid Nitrogen temperature (LNT). All spectra are corretted for CL spectrometer system response.

WDS analysis

WDS electron microprobe analyses were performed with a JEOL JXA 8600 superprobe at 15 kV and 200 nA of probe current. REE were detected using Lα or Lβ lines. All other elements (P, Si, Ca, F, Th) using K or M lines. Different counting times were selected. Synthetic REE glasses (Jarosewich and Boatner,1991), pure elements and natural minerals were used as primary standards. A ZAF matrix correction routine was applied. Si and most HREE resulted below EPMA detection limit and therefore they are not reported.

LA-ICPMS analysis

Analyses by Laser Ablation - Inductively Coupled Plasma Mass Spectrometry (LA-ICPMS) were carried out at the Dipartimento di Scienze della Terra, SMAArt facilities (University of Perugia). The laser ablation system was a commercial New Wave UP213 (New Wave, UK) frequency quintupled Nd:YAG laser, whose fundamental wavelength of 1064 nm was converted into 213 nm by means of three harmonic generators. The ICP-MS instrument was a Thermo Electron X7 from Thermo Electron Corporation (Waltham, USA), a quadrupole based ICP-MS with a sensitivity better than $6x10^7$ counts per second (cps) for 1 μg ml^{-1} of indium when used in the standard solution nebulization mode.

The LA-ICPMS system was optimized for dry plasma conditions prior to each analytical session on a continuous linear ablation of NIST SRM 612 by maximizing the signals for selected masses (La$^+$ and Th$^+$) and reducing oxide formation by minimizing the ThO$^+$/Th$^+$ ratio. Helium was preferred over argon as a carrier gas to

enhance the transport efficiency of ablated material (Eggins et al., 1998). The helium carrier gas was mixed with argon make-up gas downstream the ablation cell and before entering the ICP torch; this configuration allows to maintain stable and optimum excitation condition. The sample was loaded along with the NIST SRM 612 glass standard and a quality control sample in the ablation cell and all measurements were carried out using time resolved analysis operating in a peak jumping mode. Data were collected in discrete runs, comprising 6-10 unknowns samples and 1 quality control standard analyzed as unknown bracketed before and after by 4 analyses of the external standard. Calibration was performed using NIST SRM 612 (Pearce et al., 1997) as external calibration sample in conjunction with internal standardization using ^{140}Ce previously determined by EPMA (e.g. Chen et al, 1997). Internal standardization was employed to correct for ablation differences resulting from different ablation condition between sample and reference material. The laser beam size, repetition rate and the laser energy density were fixed to 20 μm, 10 Hz and ~10 J/cm^2 respectively. Table 1 provides a compilation of instrument and data acquisition parameters for LA-ICPMS analysis. Figures of merits (limits of detection, precision, accuracy) achieved under the operating conditions described above were determined on the USGS BCR2G basalt glass standard (USGS, 2005) and are reported in Table 2. The results obtained for the USGS BCR2G basalt glass standard by Norman et al. (1998), Gao et al. (2001), Eggins (2003) and Tiepolo et al.(2003) are also reported in Table 2. Limits Of Detection (LOD) are comprised from a maximum of 500 ppm for Si and a minimum of 0.008 ppm for U and decrease as the mass to charge increases. Precision and accuracy, calculated as Relative Standard Deviation (RSD) and deviation from the reference value respectively, are always below 10 % (Table 2) .

LA-ICPMS analyses of minor and trace elements on monazite samples show RSD values below 10% for Sr, Y, Th, and HREE while other elements give slightly higher RSD (Table 4).

RESULTS AND DISCUSSION

Sample selection and description

The studied monazite occurs in the altered rim of a metre-thick hydrothermal vein intruded in the *Scisti Grafitici* Unit of the Dora Maira Massif (Italian Western Alps) cropping out south of Bocciarda Mtn., on the left side of Val Chisone (TO).

This vein shows a mineralogical zoning, being mostly composed of quartz in the middle portion and albite in the outer rim. K-feldspar, sericite, rutile (the latter concentrated along the contact between vein and wallrock), green biotite and sulfides (arsenopyrite, pyrite, pyrrhotite, galena and chalcopyrite) also occur in very low amount. At the contact with the vein the host graphitic schists show enrichments in albite, quartz, sericite and – as accessory phases – monazite, zircon, rutile, apatite, thorite, huttonite and sulfides (arsenopyrite, pyrite, pyrrhotite, galena and chalcopyrite). Monazite in included in albite.

Four monazite crystals (hereafter MON1-MON4) with a size > 50 μm were identified and selected by optical and electron microscopy (Fig. 1). These crystals were carefully observed by SEM-BSE and CL panchromatic and monochromatic images. The areas showing different CL intensity were first investigated by CL spectra, furthermore WDS electron microprobe analyses were carried out. The same areas were finally analysed by LA-ICPMS facility.

SEM/BSE and CL preliminary investigation

The monazite crystals occurring at the border of the sampled vein, once identified by optical and BSE images were selected for the CL and micro-chemical study.

SEM/BSE images were firstly performed on 4 selected monazite crystals in order to attest the sample homogeneity or to evidence chemical zoning in major elements. Fig. 1 reports the selected crystals and shows that no patchy or evident chemical zoning occur.

CL panchromatic and monochromatic images were performed on all 4 selected monazite crystals in order to evidence and map different whole CL properties. Fig. 2 shows the panchromatic image of MON4 and the monochromatic (at 330nm) image of MON1 (the bigger crystals) indicating that both crystals are characterized by darker and lighter areas (i.e. more or less luminescent areas) in both panchromatic and monochromatic conditions. These interesting areas underwent a preliminary CL spectra investigation at room temperature.

CL spectra performed in both darker and lighter areas of all 4 monazite crystals, reported in Fig. 3, show three broad bands centered at 332, 634 and 683 nm, respectively. In table 5, the centroid mean value and the mean Full Width Half Maximum (FWHM) obtained by a gaussian fitting on MON1 and MON4 spectra, are reported with the mean value and the relative standard deviations (σ).

6

It has to pointed out the followings: i) the smaller monazites supply considerable lower CL intensities in spite of using the same analytical conditions (i.e. probe current, kV, WD and resolution); ii) the darker areas have lower CL intensities with respect to the lighter ones. iii) the spectra acquired in two lighter areas of the same crystal, both in the core and the rim, have the same CL intensity; iiii) a comparable whole CL intensity is shown by the two bigger crystals, if the darker and lighter areas are considered separately; iiiii) the same CL intensity characterizes the smaller crystals.

On the whole, these spectra suggest that different CL intensities are produced by different portions of the selected crystals and that, at least, three broad bands occur. Therefore, a more detailed CL investigation at higher resolution is necessary to solve the main broad bands and to discriminate minor peaks occurring in between.

Microchemical investigation

A representative set of EPMA and LA-ICPMS data, purposely performed in both darker and lighter CL areas, are reported in table 3 and 4, respectively.

The studied monazite is a "normal" Ce-monazite according to Foster (1998), with a mostly homogeneous major element (Ce, La, Nd, Pr, Sm, Eu and Gd) composition (Fig. 4). Si, Th, Y, and Dy are also present as minor elements at thousand ppm values (Fig. 5). Most trace elements (Tb, Ho, Er, Al, Ca, Sr and U) occur at hundreds ppm level; only few ppm of Pb and of the highest HREEs are detected.

Taking into account the bigger monazite crystals (MON1 and MON4), whose CL intensities are significantly higher, and plotting the major, minor and trace element compositions of darker and lighter CL areas it is clear that no relevant or systematic chemical difference exists between the two portions of the single crystal. However, all minor elements (Si, Th, Ca and Y) result clearly the most variable elements together with U but the differences do not seem to be systematic or related to different CL intensities.

CL Spectra

CL spectra on the selected monazite were again carried out with a resolution of 1 nm in order to detail the whole region of spectrum and to discriminate minor and major peaks at higher resolution. Both darker and lighter areas were investigated in MON1 and MON4 (Fig. 6). The results of MON4 – the same is for MON1 - are shown in

7

Fig. 7. These CL spectra confirm the occurrence of three main broad-bands similarly centred and suggest the occurrence of some narrow superimposed peaks. In addition, two minor peaks are recognizable at about 380 and 490nm.

In Fig. 8a, the CL spectrum (SPAn#3) performed on An#3 of MON4 crystal, with previous reported analytical conditions, but acquired at LNT, is displayed. The gaussian fitting of SPAn#3 shown in Fig.8.b suggests that Broad band I is made up of two components centred at 316 and 339 nm (peaks 1 and 2 in Table 6): on the right tail of this band two peaks are also recognizable at 385 and 411 nm (peaks 3 and 4 in Table 6). At higher wavelengths two further peaks occur at 485 and 498 nm (peaks 5 and 6 in Table 6).

In Fig. 8c, on the left tail of Broad band II, are visible two peaks centred at 562 and 596 nm (peaks 7 and 8 in Table 6). Finally, peaks 9 and 10 of Table 6 correspond to the two already cited overlapping bands (II and III) centred at 634 and 682 nm.

Comparing the broad band centroids with previous literature data on luminescence on phosphates we can tentatively attribute the first two bands (Gorobets, 2002 and reference therein) to Gd^{3+} and Ce^{3+}, respectively, but we are unable to solve the two broad bands at higher wavelength.

Minor peaks which may be ascribed to the presence of Tb^{3+}, Dy^{3+} and Sm^{3+} (Fig. 8b-c) as supported by literature data on REE electronic transitions producing luminescence on phosphates (Gorobetz, 2002, Marfunin, 1979) and fortifying by the minerochemical data which confirmed the presence of Tb, Dy and Sm as trace or minor element. Only one minor peak centred at 498 nm remains unsolved.

In LAP phosphors (LaPO$_4$: Ce^{3+},Tb^{3+} - monoclinic monazite type structure), it is well-known a luminescence mechanism where a strong energy transport from sensitizer (Ce^{3+}) to activator (Tb^{3+}), in some cases with assistance of Gd^{3+}, exists (Srivastava and Ronda, 2003). However, this phosphors behaviour happens if Tb concentration is two order of magnitude greater (8÷9 wt%) than in the studied monazites where Tb is present as trace element (< 1000 ppm). In our case, as Tb peaks are weak, a small transfer of energy towards Tb is supposed to occur and, therefore, Ce^{3+} and Gd^{3+} luminesce is more intense and compatible with our results.

CONCLUSIONS

1) *in situ* microchemical analyses on monazite crystals from Dora Maira Massif veinlet indicate Ce-rich compositions, with mostly homogeneous values of

LREE and more variable HREE: the latter occurring as minor or trace elements together with Th, U, Y , Ca and Sr.

2) CL panchromatic and monochromatic images on selected crystals evidence the occurrence of darker and lighter areas (i.e. more or less luminescent crystal portions) indicating that different parts of a single crystal have a different luminescent response not clearly related to difference in chemical activators .

3) High resolution CL spectra performed at room and liquid nitrogen temperature indicate that the main luminescence response is due to four bands, partially overlapping. These four bands, centered at 316, 339, 634 and 683 nm have a width of several nm and a common variable intensity if the darker and lighter crystal portions are considered separately. The two first bands may be tentatively due to Gd^{3+} and Ce^{3+}, respectively. The broad bands at higher wavelength remain unsolved.

4) Six minor peaks occur in the region between the two main band pairs. These CL peaks (except one) may be presumably correlated to the presence of Tb^{3+}, Dy^{3+} and Sm^{3+} as activators.

REFERENCE

Chen Z., Doherty W., and Conrad D.G. (1997). Application of laser sampling microprobe inductively coupled plasma mass spectrometry to the in situ trace element analysis of selected geological materials. Journal of Analytical Atomic Spectrometry 12, 653-659.

Cherniak D. J., Watson E.B., Grove M., Harrison T. M. (2004). Pb diffusion in monazite: a combined RBS/SIMS study. Geochim. Cosmochim. Acta, 68, 829-840.

Egging S.M (2003) Laser ablation ICP-MS analysis of geological materials prepared as lithium borate glasses. Geostandards Newsletter **27**, 147-162.

Egging S.M., Kinsley L.P.J. and Shelley J.M.G. (1998). Deposition and element fractionation processes during atmospheric pressure laser sampling for analysis by ICP-MS. Applied Surface Sciences 127-129, 278-286.

Foster H. J. (1998). The chemical composition of REE-Y-Th-Urich accessory minerals in peraluminous granites of Erzgebirge-Fichtebirge region, Germany, Part I: The monazite-(Ce)-brabantite solid solution series. Am. Mineral., 83: 259-272.

Gao S., Xiaomin L., Yuan H., Hattendorf B., Günther D., Chen L. and Hu S. (2002). Determination of forty two major and trace elements in USGS and NIST SRM glasses by laser ablation-inductively coupled plasma-mass spectrometry. Geostandards Newsletter 26, 181-196.

Gorobets B. S. and Rogojine A. A. (2002). Luminescent spectra of minerals: reference book. Moscow 2002, 300 pp.

Govindaraju K. (1994). 1994 compilation of working values and sample description for 383 geostandards. Geostandards Newsletter 18, 1-158.

Harrison T. M., Catlos E. J. and Motel J. M. (2002). U-Th-Pb dating of phosphates. In Phosphates: Geochemical, geobiological and materials importance. Reviews in Mineralogy and Geochemistry, 48, 523-558. Mineralogical Society of America.

Jarosewich E., Boatner L.A.,1991: Geostandards Newletter, 15, 397-399.

Longerich H.P., Jackson S.E. and Günther D. (1996). Laser ablation-indictively coupled plasma mass spectrometric transient signal data acquisition and analyze concentration calculation. Journal of Analytical Atomic Spectrometry 11, 899-904.

Norman M.D., Griffin W.L., Pearson N.J., Garcia M.O. and O'Reilly S.Y. (1998). Quantitative analysis of trace elements abundances in glasses and minerals: a comparison of laser ablation inductively coupled plasma mass spectrometry, solution

inductively coupled plasma mass spectrometry, proton microprobe and electron microprobe data. Journal of Analytical Atomic Spectrometry 13, 477-482.

Marfunin A.S. (1979). Spectroscopy, Luminescemce and Radiation Centers in minerals. Springer-Verlag, Berlin, Hiedelber New York, 1979, 352 pp.

Parrish R. (1990). U-Pb dating of monazite and its application to geological problems. Can. J. Earth Sci., 17, 1431-1450.

Petrelli M., Caricchi L., e Ulmer P. (2005). Application of High Spatial Resolution Laser Ablation ICP-MS to Crystal-Melt Trace Element Partition Coefficient Determination. In prep.

Remond G.,Phillips M.R., Roques-Carmes C. (2000). "Importance of Instrumental and Experimental Factors on the Interpretation of Cathodoluminescence Data from Wide Band Gap Materials" in "Cathodoluminescence in Geoscience" Pagel M., Barbin V., Blanc P., Ohnenstetter D. eds. 59-126.

Spear F. S. & Pyle J. M. (2002). Apatite, monazite and xenotime in metamorphic rocks. In: Phosphates, Reviews in Mineralogy and Geochemistry, Vol 48: 293-335.

Srivastava A.M. and Ronda C. R. (2003). Phosphors. The Electrochemical Society Interface – Summer 2003, 48-51.

Suzuki K., Adachi M. and Kazjizuka I. (1994). Electron microprobe observation of Pb diffusion in metamorphosed detrital monazite. Earth Planet. Sci. Lett., 128: 391-405.

Tiepolo M., Bottazzi P., Palenzona M. and Vannucci R. (2003). A laser probe couplet with ICP-double focusing sector-field mass spectrometer for in situ analysis of geological samples and U-Pb dating of zircon. The Canadian Mineralogist 41, 259-272.

USGS (2005). Geochemical reference material and certificates. http://minerals.cr.usgs.gov/geo_chem_stand/.

FIGURE CAPTIONS

Fig. 1 – Backscattered electron images of MON1-MON4 monazite crystals.

Fig. 2 – 2a) panchromatic CL image of MON4; 2b) Monochromatic (340 nm) CL image of MON1.

Fig. 3 – CL spectra of MON1-MON4 monazites carried out in both darker and lighter areas.

Fig. 4 – Hystogram of major (4a) and minor (4b) elements composition of MON1 and MON4 crystals determined by EPMA analysis. D = darker CL area; L = Light CL area.

Fig. 5 - Hystogram of most minor and trace elements in MON1 and MON4 crystals determined by LA-ICPMS analysis. D = darker CL area; L = Light CL area. # = number of analysis.

Fig. 6 – BSE image of MON4 showing the location An#3, An#4 and An#5 reported in Table3 and the location of CL spectra of Fig. 7 (SPAn#3, SPAn#4, SPAn#5). SPAn#3 = CL spectrum in An#3 location area etc.

Fig. 7 – CL spectra of MON4 performed at room temperature and nm resolution in both darker and lighter areas shown in Fig. 6.

Fig. 8 – a) LNT CL spectra of MON4 performed on AN#3 spot area; b) Gaussian fitting of the spectrum from 300 to 550 nm; c) Gaussian fitting of the spectrum from 550 to 800 nm.

TABLE CAPTIONS

Table 1 - Laser Ablation and ICPMS operation condition.

Table 2 - Figures of merit determined on the USGS glass reference standard. All concentration values are in ppm. [a] Nb, Dy and Er values are form Govindaraju (1994) and remainder of the elements are from USGS (2006), [b] Al, Si, Ca, Ti and Mn determined by EPMA and remainder of the elements by LA-ICPMS.

Table 3 – Representative EPMA analyses of monazite samples. Major elements expressed as wt.% oxide. D = darker CL area; L = Light CL area. # = Number of analysis.

Table 4 – LA-ICPMS minor and trace elements of monazite crystals expressed as ppm. D = darker CL area; L = Light CL area. An# = Number of analysis. σ = standard deviation.

Table 5 – Band centroid and FWHM calculated on MON1 and MON4 spectra of Fig. 3. The mean values (Mean) and the standard deviation (σ) are calculated on all the displayed spectra of Fig 3. # = number of analysis reported on Table3; D = dark area; L = light area.

Table 6 – Gaussian fitting of SPAn#3 spectrum displayed in Fig. 8a. All determined centroid with the relative FWHM are reported.
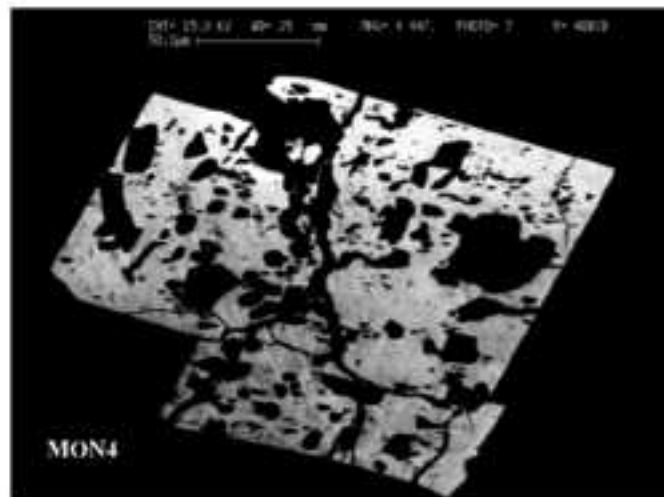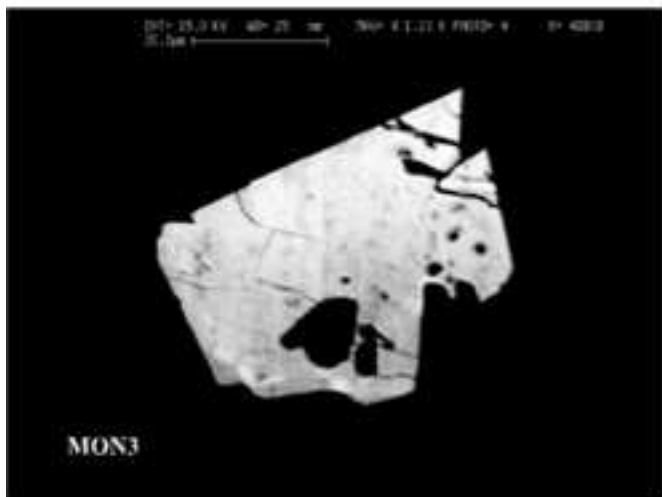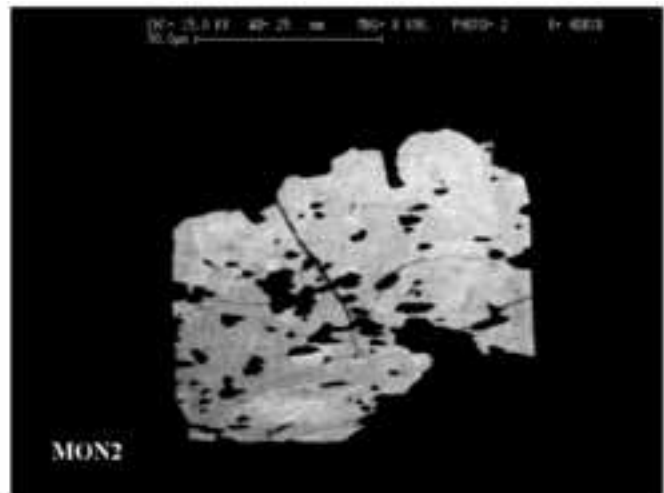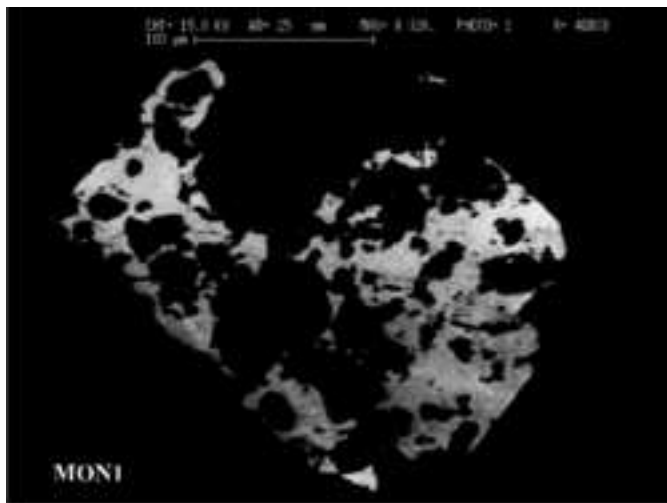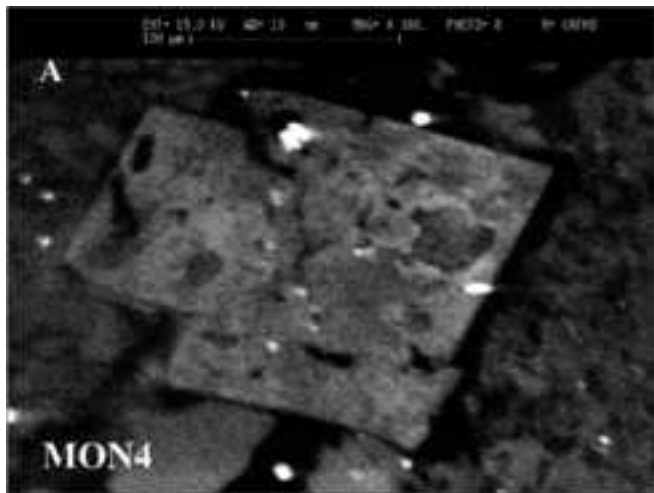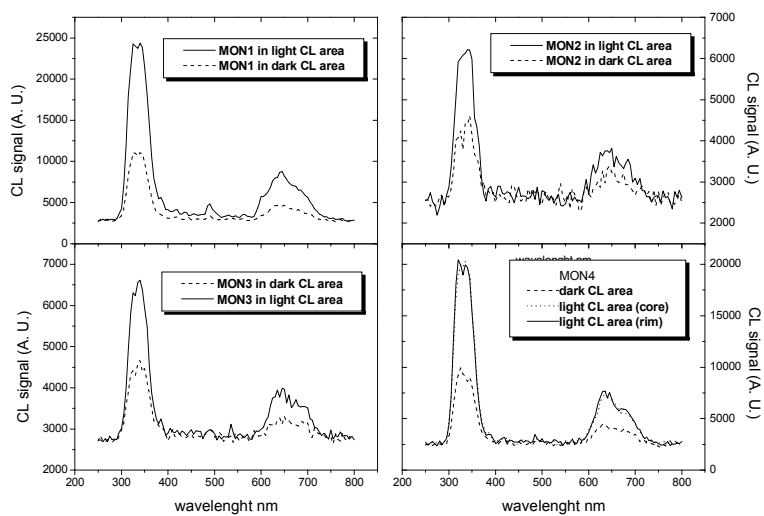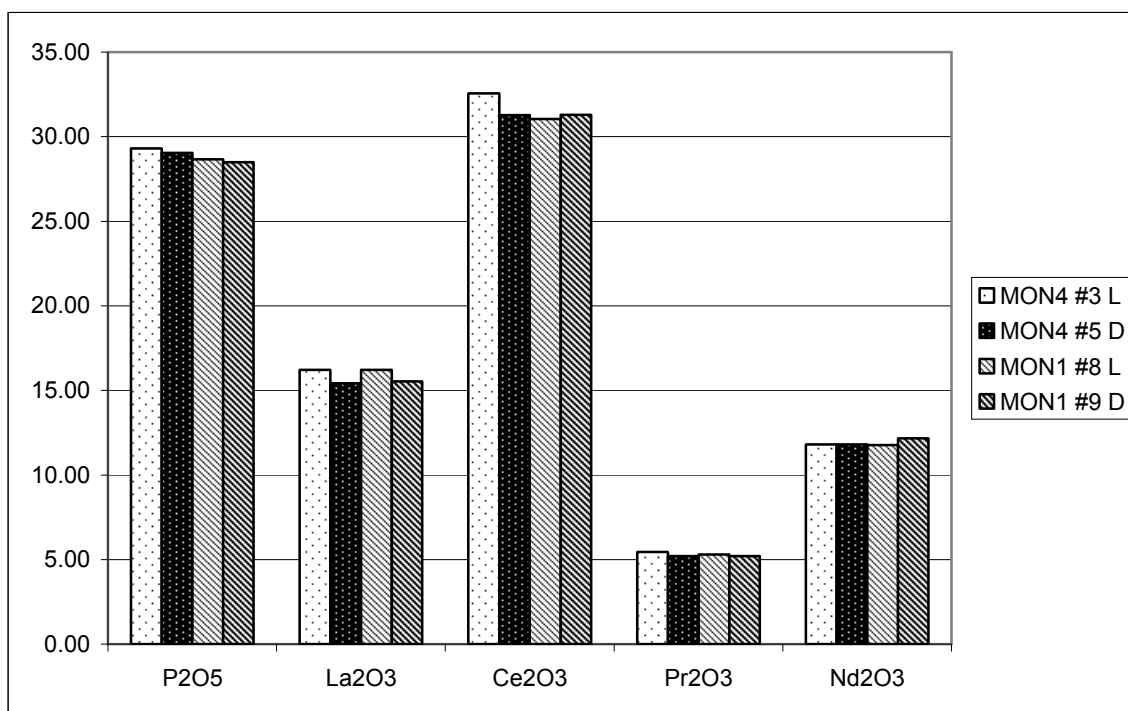
Fig. 1

Fig. 2

Figure

Fig. 3
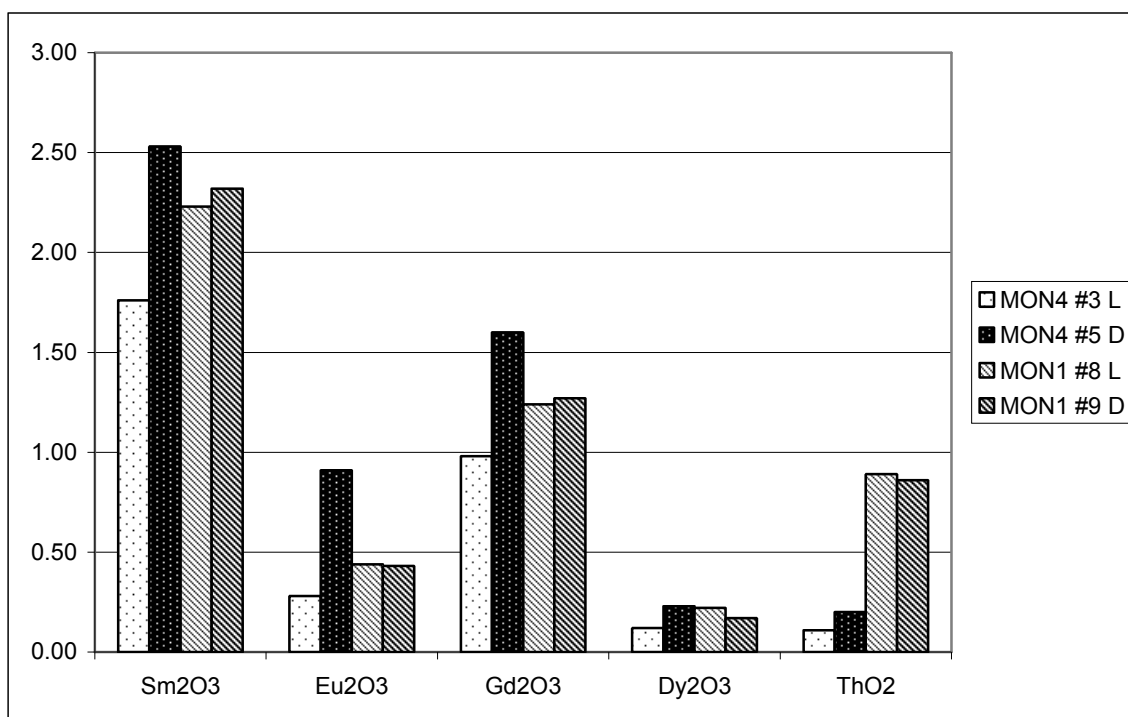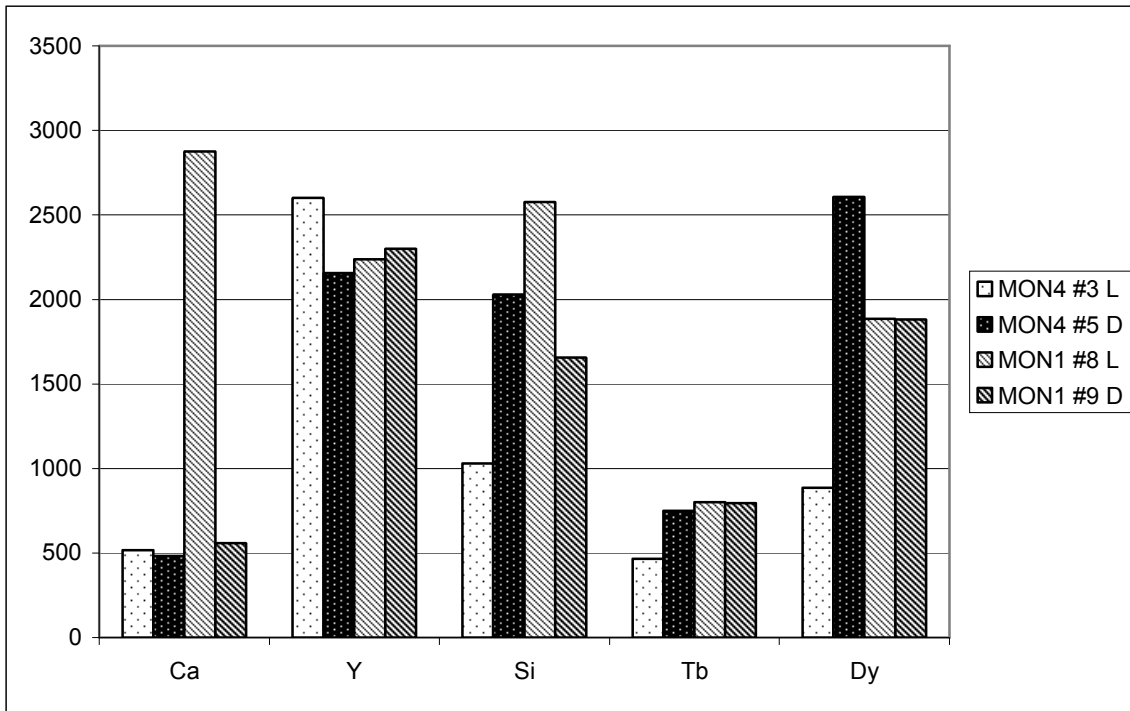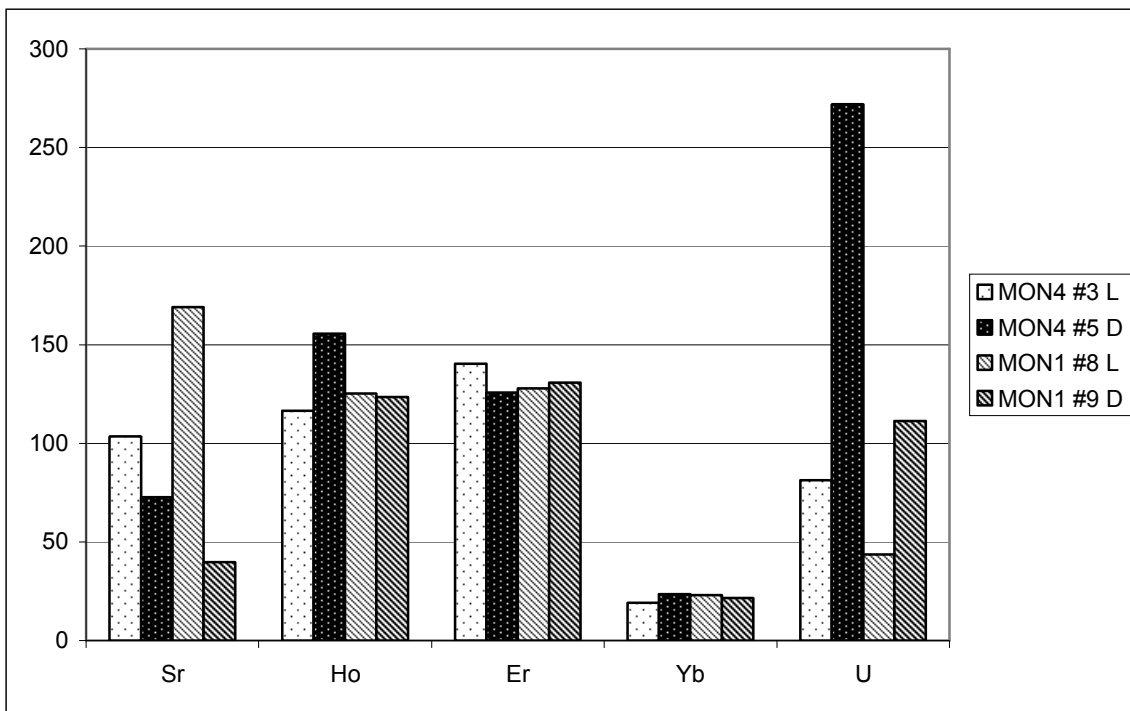
Figure
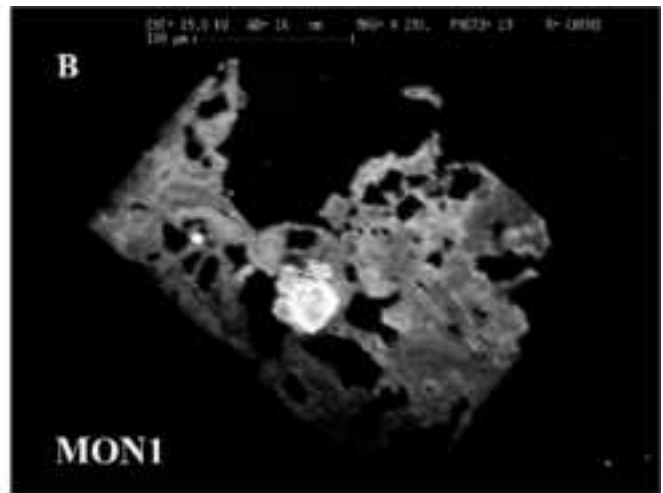
Fig. 4a EPMA Major elements

Fig. 4b EPMA minor elements

Fig. 5 – LA-ICPMS minor and trace elements

L= SE1   EHT= 30.0 KV   WD= 19   mm   MAG= X 346.   PHOTO= 7
100 µm

An# 5

An# 3

An# 4

Fig. 6

Figure
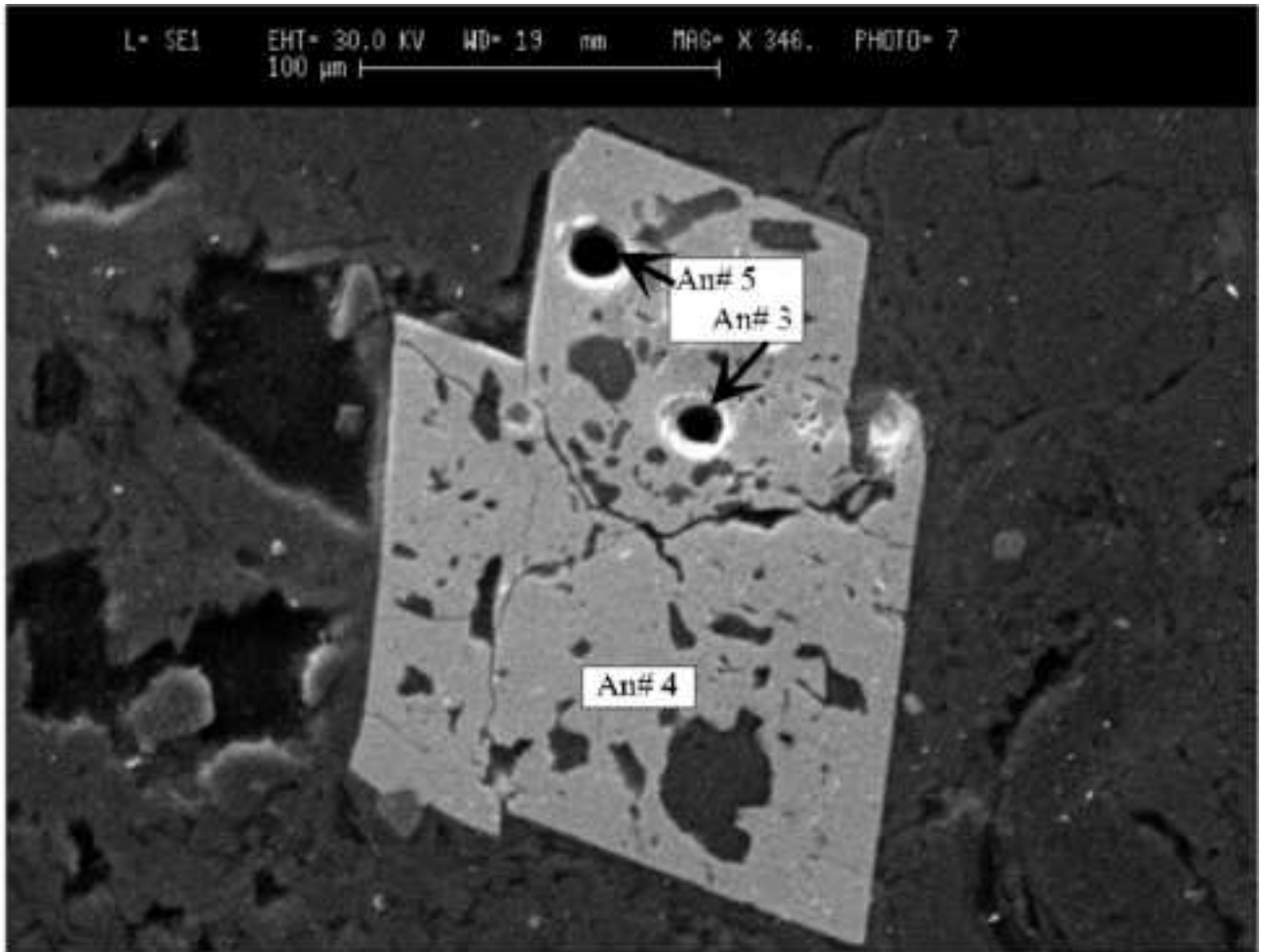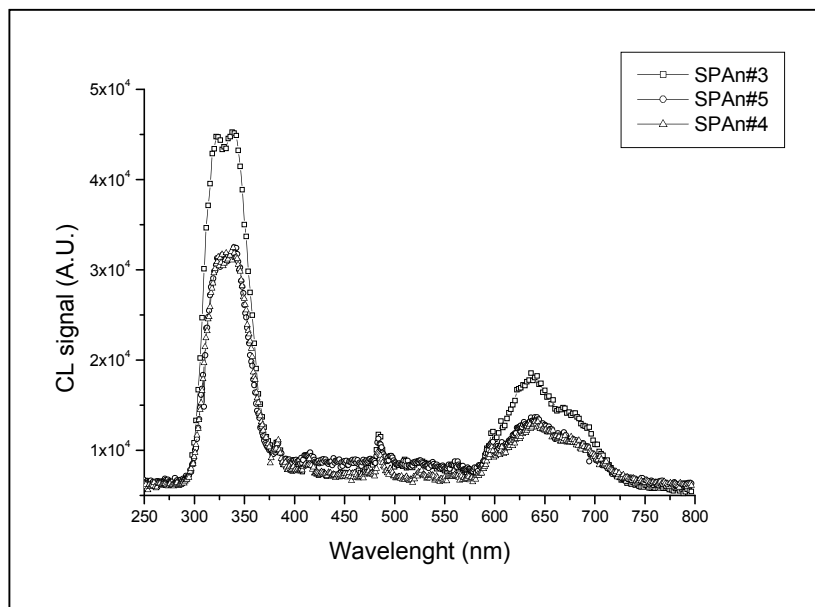
Fig. 7

Fig. 8a

Fig. 8b – 8c

Fig. 9

Figure

Fig. 10

Table

Plasma condition		
RF Power	1200-1250 W	
Plasma Gas Flow	14 l min^{-1}	
Auxiliary Gas Flow	0.95 l min^{-1}	
Helium Carrier Gas Flow	0.76 l min^{-1}	
Argon Make Up Gas Flow	0.76 l min^{-1}	
Data Acquisition Parameters		
Scanning Mode	Peak hopping	
Dwell Time	25 ms	
Background Acquisition Time	40 s	
Signal Acquisition Time	40 s	
Elements Scanner	^{27}Al, ^{29}Si, ^{42}Ca, ^{47}Ti, ^{51}V, ^{55}Mn, ^{85}Rb, ^{88}Sr, ^{89}Y, ^{90}Zr, ^{93}Nb, ^{137}Ba, ^{159}Tb, ^{163}Dy, ^{165}Ho, ^{166}Er, ^{169}Tm, ^{173}Yb, ^{175}Lu, ^{178}Hf, ^{208}Pb, ^{232}Th, ^{238}U	
Laser Ablation		
Laser Ablation device	New Wave UP213	
Laser Type	Nd-YAG	
Wavelength	213 µm	
Mode	Q-Switched	
Shot Repetition Rate	10 Hz	
Energy Density on Sample Surface	~ 10 J cm^{-1}	
Spot Diameter	20 µm	

Table1- Laser Ablation and ICPMS operation condition

Table

Table 2 - Figures of merit determined on the USGS glass reference standard. All concentration values are in ppm. [a] Nb, Dy and Er values are form Govindaraju (1994) and remainder of the elements are from USGS (2006), [b] Al, Si, Ca, Ti and Mn determined by EPMA and remainder of the elements by LA-ICPMS.

Element	Isotope	This Study (n=5)	Average LOD (n=5)	RSD % (n=5)	Accuracy% (n=5)	BCR2[a] USGS (2006), Govindaraju (1994)	BCR2-G[b] Norman et al. (1998)	BCR2-G Gao et al. (2001)	BCR2-G Eggins (2003)	BCR2-G Tiepolo et al. (2003)
Al	27	78000	25	9.9	9.2	71400	72000	-	-	-
Si	29	271000	500	9.3	7.1	253000	254200	-	-	-
Ca	42	52800	250	4.5	3.7	50900	50900	-	-	-
Ti	47	14400	15	9.9	6.7	13500	13700	13005	13803	-
V	51	432.33	1.2	7.2	3.9	416	414	425	427	451
Mn	55	1568	2	8.9	3.1	1520	1549	1463	-	-
Rb	85	45.6	0.6	7.7	-5.1	48	49	51	46.1	51.3
Sr	88	358	0.4	7.5	3.6	346	342	321	338	352
Y	89	37	0.20	5.4	0.5	37	35.3	31	36.2	34.3
Zr	90	194	0.9	6.2	3.4	188	194	167	191.5	197
Nb	93	14.1	0.2	7.1	0.7	14	12.8	10.9	12.77	14.8
Ba	137	703	0.9	8.1	2.9	683	660	641	662	717
Tb	159	0.98	0.02	9.2	-8.4	1.07	-	0.95	-	1.0
Dy	163	6.3	0.14	7.9	-0.6	6.34	6.5	6.0	6.18	6.3
Ho	165	1.4	0.03	7.1	5.3	1.33	1.31	1.2	-	1.3
Er	166	3.8	0.10	7.9	4.7	3.63	3.6	3.3	3.6	3.6
Tm	169	0.50	0.04	6.0	-7.4	0.54	-	0.46	-	0.5
Yb	173	3.3	0.21	9.1	-5.7	3.5	3.5	3.2	3.32	3.4
Lu	175	0.54	0.03	9.3	5.9	0.51	0.51	0.47	0.50	0.5
Hf	178	5.2	0.08	5.8	8.3	4.8	5	4.5	4.74	4.8
Pb	208	9.9	0.07	5.1	-10.0	11	11.5	11	10.3	11.5
Th	232	6.4	0.020	4.7	3.2	6.2	6.1	5.5	5.72	6.2
U	238	1.6	0.008	6.3	-5.3	1.69	1.73	1.7	1.58	1.9

Table

Table 3 - Representative EPMA analyses of monazite samples. Major elements expressed as wt.% oxide. D = darker CL area; L = Light CL area. # = Number of analysis.

SAMPLE	MON4			MON1		MON2	MON3
An#	#3	#4	#5	#8	#9	#10	#14
	L	D	D	L	D	D	L
P_2O_5	29.31	28.45	29.05	28.67	28.49	29.09	29.01
La_2O_3	16.22	14.31	15.43	16.23	15.54	14.07	16.08
Ce_2O_3	32.57	31.31	31.28	31.04	31.29	30.83	31.23
Pr_2O_3	5.45	6.67	5.22	5.31	5.22	5.83	5.45
Nd_2O_3	11.81	13.21	11.81	11.77	12.16	13.18	11.89
Sm_2O_3	1.76	2.20	2.53	2.23	2.32	2.51	2.33
Eu_2O_3	0.28	0.15	0.91	0.44	0.43	0.12	0.42
Gd_2O_3	0.98	1.2	1.60	1.24	1.27	1.59	1.45
Dy_2O_3	0.12	0.21	0.23	0.22	0.17	0.34	0.34
ThO_2	0.11	0.86	0.20	0.89	0.86	0.22	0.06
CaO	0.07	0.24	0.08	0.16	0.08	0.13	0.11
Y_2O_3	0.22	0.4	0.30	0.29	0.31	0.57	0.35
F	0.31	0.4	0.32	0.36	0.34	0.37	0.29
Total	99.21	99.61	98.96	98.85	98.48	98.85	99.01
P	1.032	1.002	1.023	1.010	1.004	0.995	1.022
La	0.238	0.210	0.227	0.241	0.232	0.207	0.237
Ce	0.474	0.456	0.457	0.457	0.463	0.449	0.457
Pr	0.079	0.097	0.076	0.078	0.077	0.085	0.079
Nd	0.167	0.188	0.168	0.169	0.176	0.187	0.170
Sm	0.024	0.030	0.035	0.031	0.032	0.034	0.032
Eu	0.004	0.002	0.012	0.006	0.006	0.002	0.006
Gd	0.013	0.015	0.021	0.017	0.017	0.021	0.019
Dy	0.002	0.003	0.003	0.003	0.002	0.004	0.004
Th	0.001	0.008	0.002	0.008	0.008	0.002	0.001
Ca	0.003	0.003	0.003	0.007	0.003	0.006	0.005
Y	0.005	0.006	0.006	0.006	0.007	0.012	0.007
Total cation*	2.041	2.020	2.035	2.032	2.026	2.004	2.038

* Compositions normalised to 4 oxygen anions

Table

Table 4 – LA-ICPMS minor and trace elements of monazite crystals expressed as ppm. D = darker CL area; L = Light CL area. An# = Number of analysis. σ = standard deviation.

Sample	MON4		MON4		MON1		MON1		MON2		MON3	
An#	#3	σ	#5	σ	#8	σ	#9	σ	#10	σ	#14	σ
	L		D		L		D		D		L	
Al	206	18	1430	89	479	30	296	19	997	62	664	41
Si	1030	356	2030	321	9576	1006	1655	214	2508	350	486	197
Ca	518	238	484	168	2876	243	558	98	662	167	473	137
Ti	42	10	36	7	560	62	134	15	133	17	26	6
V	bdl		bdl		1.6	0.6	bdl		13.7	1.06	bdl	
Mn	bdl		bdl		6.8	0.85	1.4	0.4	4.5	0.82	0.9	0.56
Rb	bdl		2.7	0.39	1.2	0.19	0.3	0.098	6.8	0.81	1.0	0.18
Sr	104	9	73	6	169	12	40	3	81	6	48	4
Y	2600	158	2156	126	2237	120	2299	121	4571	252	2003	114
Zr	bdl		bdl		3.4	0.4	0.7	0.2	0.5	0.4	bdl	
Nb	bdl		bdl		1.4	0.2	0.1	0.1	bdl		bdl	
Ba	bdl	0.89	2.5	0.7	3.9	0.56	bdl	0.32	4.6	0.76	3.7	0.62
Tb	466	29	751	45	801	44	796	43	1425	81	861	50
Dy	886	82	2606	230	1884	149	1881	144	3465	283	1968	167
Ho	117	7	156	9	125	6	124	6	218	12	123	7
Er	140	7	126	6	128	5	131	5	217	9	128	6
Tm	5.9	0.4	4.2	0.3	5.5	0.3	5.6	0.3	12.3	0.6	5.7	0.3
Yb	19.2	1.4	23.5	1.3	23.2	1.1	21.6	1.0	60.2	2.8	25.1	1.3
Lu	1.1	0.1	1.2	0.1	1.1	0.1	1.1	0.1	3.3	0.2	1.0	0.1
Hf	0.61	0.19	0.96	0.18	0.78	0.11	0.73	0.10	1.15	0.18	0.96	0.15
Pb	4.6	0.4	2.9	0.2	15.0	0.9	6.5	0.4	3.0	0.2	1.8	0.2
Th	1526	115	1071	78	8863	581	3787	242	1730	117	634	44
U	81	11	272	34	44	5	111	12	49	6	58	7

Table 5 – Band centroid and FWHM calculated on MON1 and MON4 spectra of Fig. 3. The mean values (Mean) and the standard deviation (σ) are calculated on all the displayed spectra of Fig. 3. # = number of analysis reported on Table3; D = dark area; L = light area.

CENTROID	Band I	Band II	Band III
MON1 #8 L	336.4	640.2	691.4
MON1 #9 D	336.1	639.1	687.9
MON4 #3 L	328.8	634.2	682.6
MON4 L	327.9	629.6	677.5
MON4 #5 D	329.4	625.8	673.5
Mean	**332.4**	**634.1**	**682.9**
σ	**3.7**	**5.1**	**6.1**
FWHM	Band I	Band II	Band III
MON1 #8 L	38.3	52.7	34.5
MON1 #9 D	37.2	45.5	35.7
MON4 #3 L	36.5	43.6	37.2
MON4 L	36.4	37.7	41.3
MON4 #5 D	38.3	36.6	45.9
Mean	**37.0**	**42.8**	**38.9**
σ	**1.0**	**5.5**	**4.0**

Table

Table 6 – Gaussian fitting of SPAn#3 spectrum displayed in Fig. 8. All determined centroid with the relative FWHM are reported.

Peak	Centroid	FWHM
1	315.6	14.2
2	339	32.6
3	384.6	10.1
4	410.8	12.3
5	484.6	9.2
6	498	11.4
7	561.9	8.2
8	596.2	13.4
9	633.7	38.8
10	682.3	47.4